Near-Infrared Observations of S 255-2 : The Heart of a Massive YSO Cluster

Itoh, Yoichi ; Tamura, Motohide ; Suto, Hiroshi ; Hayashi, Saeko S. ; Murakawa, Koji ; Oasa, Yumiko ; Nakajima, Yasushi ; Kaifu, Norio ;…

(Citation)
Publications of the Astronomical Society of Japan,53(3):495-500

(Issue Date)
2001-06-25

(Resource Type)
journal article

(Version)
Version of Record

(URL)
https://hdl.handle.net/20.500.14094/90001438

PASJ: Publ. Astron. Soc. Japan **53**, 495–500, 2001 June 25

Near-Infrared Observations of S 255-2 : The Heart of a Massive YSO Cluster

Yoichi ITOH,[1] Motohide TAMURA,[2] Hiroshi SUTO,[1] Saeko S. HAYASHI,[1] Koji MURAKAWA,[3]
Yumiko OASA,[4] Yasushi NAKAJIMA,[5] Norio KAIFU,[2] George KOSUGI,[1] Tomonori USUDA,[1] and Yoshiyuki DOI[1]
[1]*Subaru Telescope, 650 N'Aohoku Place, Hilo, HI 96720, USA*
yitoh@naoj.org
[2]*National Astronomical Observatory of Japan, 2-21-1 Osawa, Mitaka, Tokyo 181-8588*
[3]*University of Hertfordshire, College Lane, Hatfield, Herts, AL10 9AB, UK*
[4]*University of Tokyo, 2-21-1 Osawa, Mitaka, Tokyo 181-8588*
[5]*Nagoya University, Furo-cho, Chikusa-ku, Nagoya, 464-8602*

(Received 2000 December 11; accepted 2001 February 22)

Abstract

High-resolution near-infrared ($JHKL'M'$) images of a massive star-forming region, S 255-2, were obtained with the Subaru Telescope and an infrared camera, CIAO. These images clearly resolve two sets of bipolar nebulae illuminated by two independent massive YSOs. A number of cluster member YSOs have been detected, including 3 new sources. Seven early-B type stars have been identified within 10 pc of S 255-2; three are associated with extended optical H II regions. The variation in the appearance of these early-B type stars suggests an evolutionary sequence of massive stars in the S 255 region.

Key words: infrared: stars — ISM: reflection nebulae — stars: formation

1. Introduction

Although we now have generally accepted pictures of low-mass star formation, the formation processes of massive stars is still uncertain. This is not simply due to the rareness of massive stars, but also due to their fast evolution. In order to investigate the massive star-formation processes, we generally compare a number of massive young stellar objects located in several massive star-forming regions. However, different massive star-forming regions have different physical parameters, such as age, distance, metallicity, and environment. Therefore, it is difficult to extract the common factors that govern the star-formation processes by studying several massive star-forming regions.

An alternative method is to study a single cluster of young stars. The cluster of optical H II regions, S 254–S 258, is an active site of massive star formation, located in the Gemini OB association (Huang, Thaddeus 1986). Several young OB stars have been discovered in these H II regions by optical photometry (Chavarría-K et al. 1987). Other signatures of massive star formation are: a peak of mm-wave CO emission located between S 255 and S 257, called S 255-2 (see Howard et al. 1997); an association with OH and H_2O masers (Turner 1971; Lo, Burke 1973); the presence of mid-infrared sources (Pipher, Soifer 1976), and CO outflows (Heyer et al. 1989). Also, S 255-2 is associated with three compact H II regions, S 255-2a, -2b, and -2c, whose exciting sources presumably correspond to B1 zero-age main sequence (ZAMS) stars (Snell, Bally 1986). All previous observations, including near-infrared imaging observations of Tamura et al. (1991), Howard et al. (1997), and Miralles et al. (1997), show evidence of massive star formation in S 255-2.

Here, we present the results of near-infrared imaging observations of the S 255-2 region with a new infrared camera on the Subaru 8.2 m telescope. Thanks to the high-quality imaging of the telescope and the instrument, we have obtained high-resolution images of S 255-2, and have resolved a number of cluster star members and bipolar nebulae.

2. Observations and Results

Near-infrared imaging observations were carried out on 2000 February 10 using the Subaru Telescope at the summit of Mauna Kea, combined with the Coronagraphic Imager with Adaptive Optics (CIAO; see Tamura et al. 2000 for the instrument details) mounted at the f/12 Cassegrain focus. The instrument was used in the direct-imaging mode (i.e. without coronagraph). An adaptive optics system was not used.

Six images were obtained through each of the J, H, K, L' ($\lambda = 3.6\,\mu$m), and M' ($\lambda = 4.7\,\mu$m) filters. The integration time for each exposure was 10 s for J, H, and K, and 3.3 s (10 co-added 0.33 s integrations) for L' and M'.

The typical FWHM of the point-spread function was $0\farcs8$ in all bands. Flat-field frames were constructed from the median-filtered images of dome-flats for J, H, and K, and using sky frames taken just after the object frames for L' and M'. The pixel scale in the "medium resolution mode" employed in our observations was measured to be $0\farcs022\,\mathrm{pixel}^{-1}$ using the Orion Trapezium cluster (Simon et al. 1999). CIAO, with a 1024×1024 pixel InSb array, yields a field of view of $22\farcs5$, in this mode. No geometric distortion was found.

The sky conditions were photometric during the observations. The near-infrared images were calibrated photometrically using the standard star, HD 40335 (Elias et al. 1982). Aperture photometry was performed using the APPHOT package in IRAF. The aperture radius was set to $1\farcs32$ for all bands.

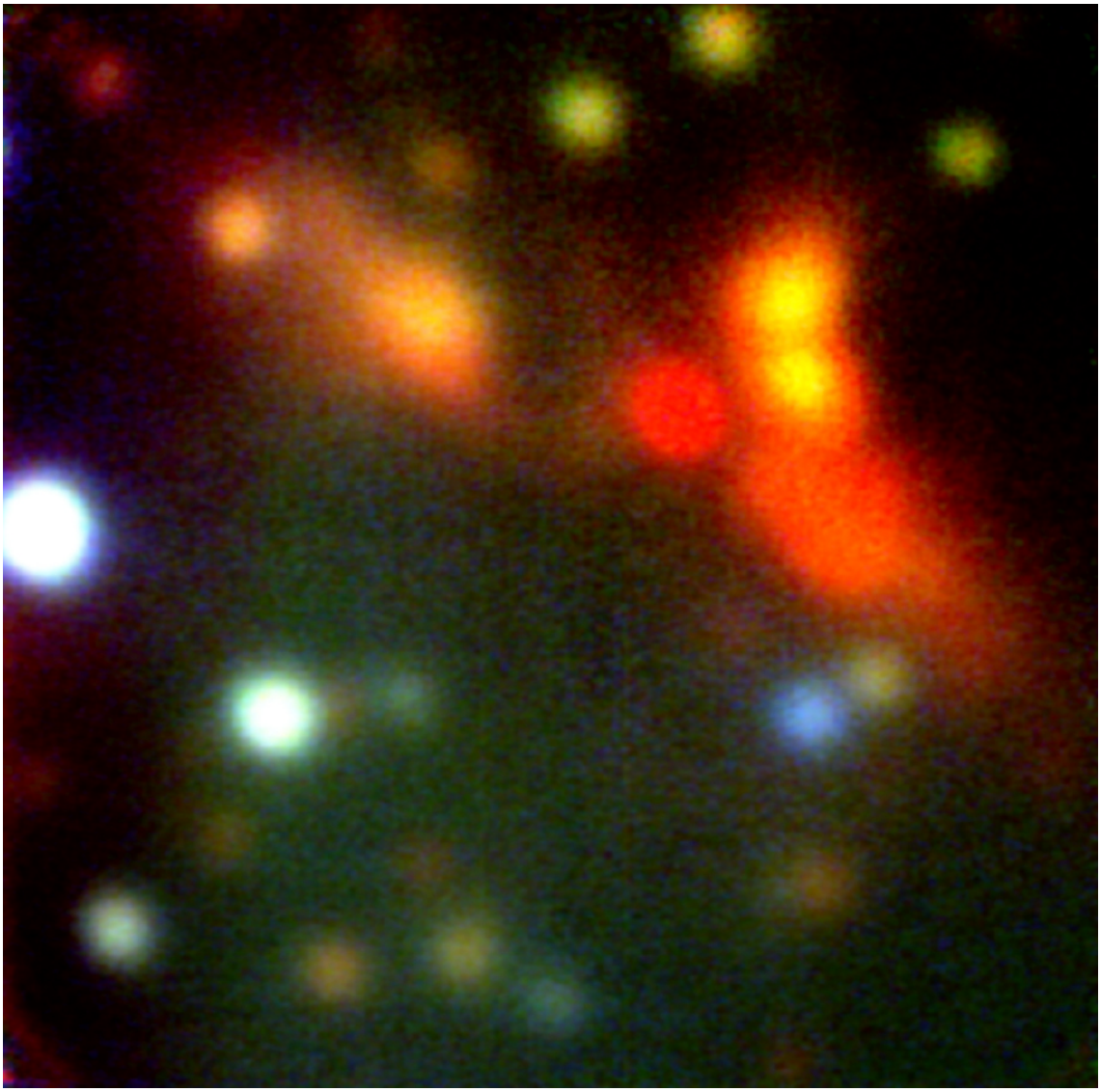

Fig. 1. JHK color composite image of S 255-2. The field of view is 22.″4. North is up, east is toward the left.

Color transformation equations between the SUBARU/CIAO system and the CIT system were derived from measurements of the "standard" standard stars and a "red" standard star in L 134 (Persson et al. 1998):

$$(J-H)_{\rm CIT} = 1.07(J-H)_{\rm CIAO}\ , \quad (1)$$

$$(H-K)_{\rm CIT} = 0.94(H-K)_{\rm CIAO}\ . \quad (2)$$

Here, we assumed that the K-band magnitudes are the same between the CIT system and the SUBARU/CIAO system. Note that the above color transformation equations were derived from only one "red" standard star. A definite equation will be presented in a following paper.

Figure 1 is a three-color composite image of S 255-2 with J (blue), H (green), and K (red). This image is the highest resolution near-infrared image of the region to date. A number of cluster sources have been detected at the J-, H-, and K-bands. It is noteworthy that the region surrounding the reddest source, NIRS 3, is clearly resolved into a point-like source and several nonstellar sources, as can be seen in this figure. Figure 2 is an L'-band contour image superposed on a K-band gray-scale image. The positions were registered between K- and L'-bands using telescope encoder values, whose accuracies are better than 1″. One source detected at both L' and M' is point-like and positionally coincident with NIRS 3, the reddest K-band source. Another $L'M'$ source is also point-like, and apparently coincident with NIRS 1.

We designated our detected sources using the nomenclature of Tamura et al. (1991) and Miralles et al. (1997). The objects NIRS 51 to NIRS 57 are not listed in Miralles et al. The positions, magnitudes, and identifications for the sources are given in table 1. All of the magnitudes have been transformed onto the CIT system. The coordinates of the objects were calculated using the coordinates of NIRS 14, NIRS 16, and NIRS 23, listed in Tamura et al. (1991). The discrepancies in the coordinates for the other objects with respect to Tamura et al. are only 0.″19 rms in both R.A. and Dec.

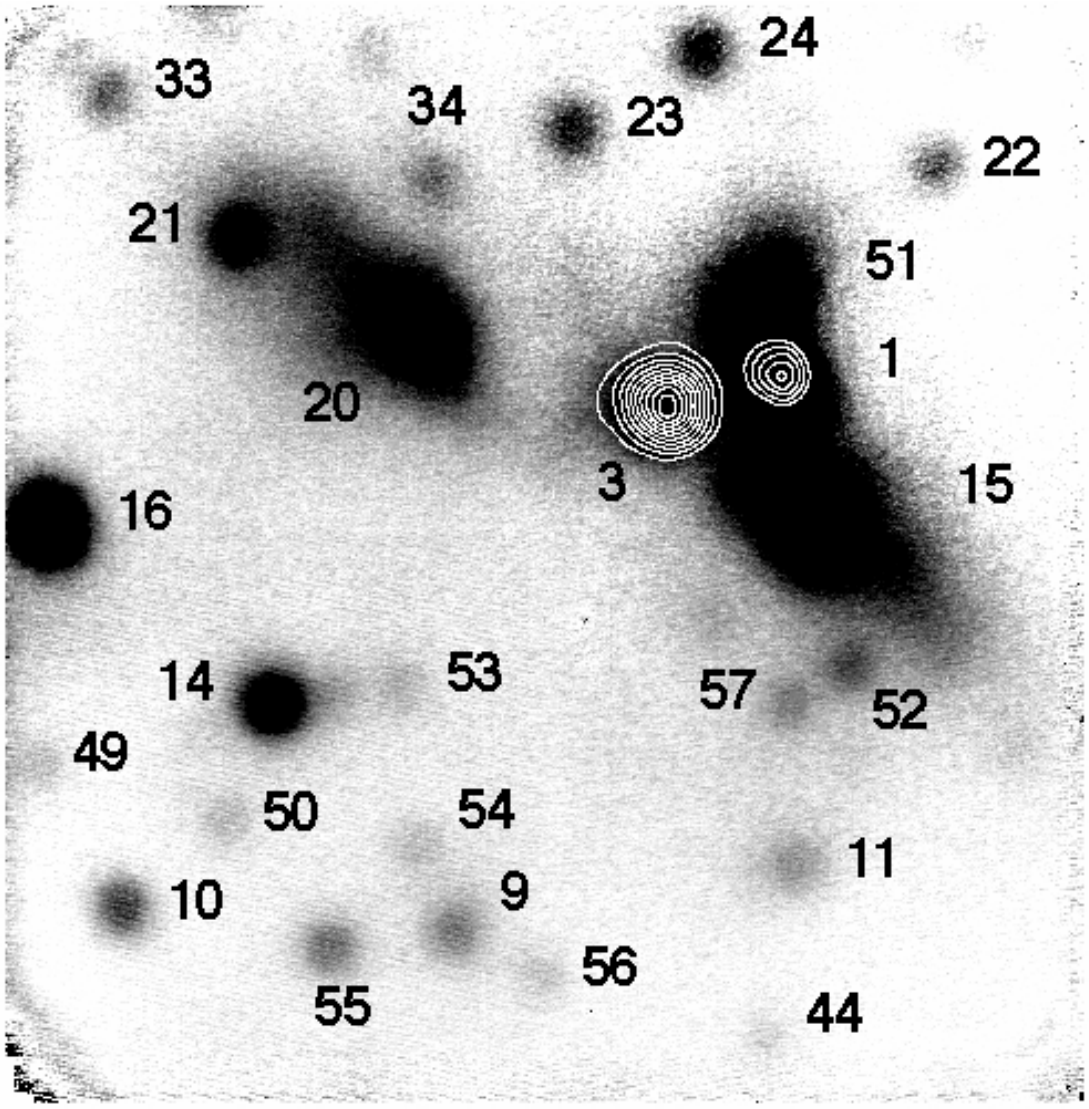

Fig. 2. L'-band contour image of S 255-2 overplotted on the K-band image. The contours are in logarithmic scale. The contour levels are $3.42 \times 10^{(-21.5+0.14i)}\,(i = 0, 1, 2...)\,\mathrm{W\,cm^{-2}\,\mu m^{-1}\,pix^{-1}}$. Each object is labeled by the NIRS number.

Our measured magnitudes are systematically fainter than the values of Miralles et al. and Howard et al. The differences are typically 0.8 mag with respect to Miralles et al. (1997), and 0.7 mag to Howard et al. (1997), for the J-, H-, and K-bands. There is no trend in the differences as a function of the brightness or color of the object. The measured magnitudes of the standard star HD 40335 are consistent with the magnitudes of other standard stars taken by CIAO on the same night. Figure 3 shows the magnitude of an isolated source, NIRS 14, as a function of the aperture radius. The instrumental magnitudes have been corrected using the magnitude of the standard star measured using the same aperture radius. The magnitudes brighten with increasing radius. Howard et al. used a $5''$ PSF fit with DAOPHOT. Miralles et al. reported that their seeing size was $\sim 1''.2$. We believe that the extended nebulosity is contributing to the measured flux for larger apertures.

The $10\,\sigma$ limiting magnitudes for our observations are 17.5, 16.5, and 16.0 for the J-, H-, and K-bands, respectively. All of the sources in the field of view found by Miralles et al. and Howard et al. have been detected. Figure 4 is a JHK color–color diagram of the objects. Due to heavy extinction, only a limited number of sources have been detected in J. It is suggested that several sources suffer from large extinction up to ~ 20 mag in this diagram. Assuming a distance of 2.4 kpc (Evans et al. 1977) and a normal extinction law (Jones et al. 1981), the foreground extinction to S 255-2 is only 0.16 mag at K. Therefore, almost all extinction appearing in figure 4 is caused by the molecular cloud S 255-2, itself.

Figure 5 is a $(K, H-K)$ color–magnitude diagram. The reddest object in the diagram is NIRS 1. (The reddest source NIRS 3 was not detected at the J- and H-bands.) The other red objects (e.g. NIRS 11, 21, 55) are mostly embedded YSOs. Their colors and magnitudes are consistent with embedded B- or A-type main-sequence stars. Some red objects are not

Table 1. $JHKL'M'$ magnitudes of sources in the S 255-2 region.

NIRS	R.A.	Dec.	J	H	K	L'	M'	Howard	Nebulosity?
1	$58^{s}.43$	$13''.07$	···	14.02 (0.01)	11.21 (0.01)	6.75 (0.01)	5.51 (0.04)	6	
3	58.61	12.53	···	···	12.01 (0.01)	5.05 (0.00)	2.74 (0.00)	7	
9	58.93	01.39	17.67 (0.11)	15.63 (0.02)	14.47 (0.01)	···	···	43	
10	59.47	02.34	15.07 (0.01)	14.61 (0.01)	13.83 (0.01)	···	···	42	
11	58.38	02.42	···	16.35 (0.04)	14.61 (0.02)	···	···	65	
14	59.23	06.60	15.01 (0.01)	13.57 (0.00)	12.86 (0.00)	···	···	37	
15	58.36	09.89	···	···	12.51 (0.01)	···	···	61	Yes
16	59.60	10.80	13.43 (0.00)	12.42 (0.00)	11.76 (0.00)	···	···	8	
20	59.01	14.68	···	14.77 (0.01)	12.65 (0.01)	···	···	30	Yes
21	59.30	16.88	17.43 (0.16)	14.86 (0.02)	13.11 (0.01)	···	···	28	
22	58.18	17.61	···	14.91 (0.02)	14.05 (0.03)	···	···	27	
23	58.77	18.80	16.73 (0.12)	14.66 (0.02)	13.66 (0.02)	···	···	26	
33	59.52	20.23	17.48 (0.21)	15.60 (0.04)	14.16 (0.02)	···	···	25	
34	58.99	17.96	···	···	14.43 (0.04)	···	···	···	
44	58.42	−01.34	···	···	15.60 (0.05)	···	···	···	
49	59.59	05.60	···	···	14.16 (0.01)	···	···	···	
50	59.31	04.14	···	···	15.47 (0.04)	···	···	···	
51	58.45	14.64	···	13.95 (0.01)	11.48 (0.01)	···	···	31	Yes
52	58.30	06.76	···	14.98 (0.02)	14.11 (0.03)	···	···	36	
53	59.04	06.88	17.62 (0.12)	15.68 (0.03)	14.74 (0.03)	···	···	···	
54	58.99	03.22	···	···	15.28 (0.04)	···	···	···	
55	59.13	01.18	18.01 (0.15)	15.85 (0.02)	14.30 (0.01)	···	···	67	
56	58.79	00.32	17.57 (0.10)	15.83 (0.03)	15.32 (0.04)	···	···	···	
57	58.39	05.95	15.64 (0.02)	14.80 (0.01)	14.38 (0.02)	···	···	38	

Note. R.A. is offset from $06^{h}00^{m}00^{s}$ (1950). Dec. is offset from $+18^{\circ}00'00''.0$ (1950).

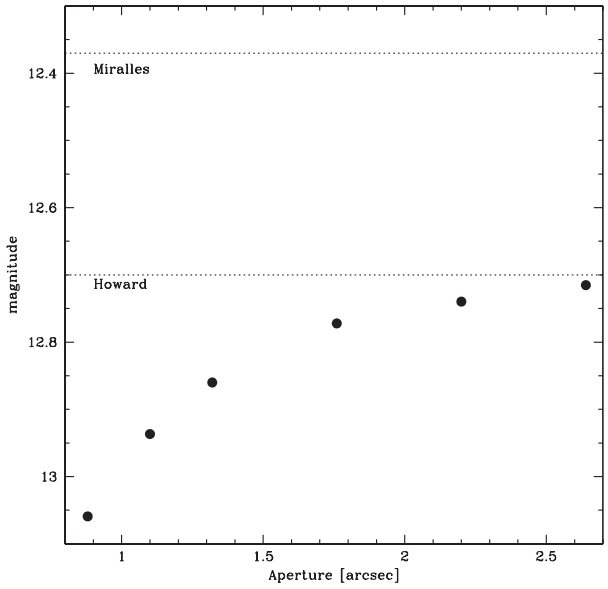

Fig. 3. Measured magnitudes of NIRS 14 as a function of the aperture radius. The magnitudes brighten with increasing radius. We used a $1''.32$ radius aperture for photometry. The magnitudes of Howard et al. (1997) and of Miralles et al. (1997) are shown by the dashed lines.

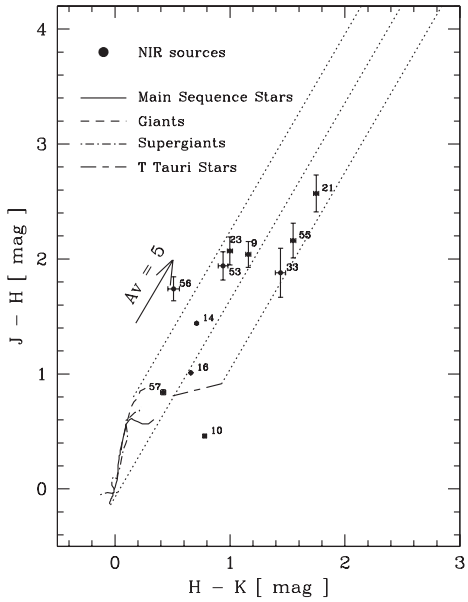

Fig. 4. Near-infrared color–color diagram of objects in the S 255-2 region. The intrinsic colors of the main-sequence stars, giants, supergiants (Tokunaga 2000), and classical T Tauri stars (Meyer et al. 1997) are indicated. The reddening vector follows Koornneef (1983). All colors are transformed onto the CIT system.

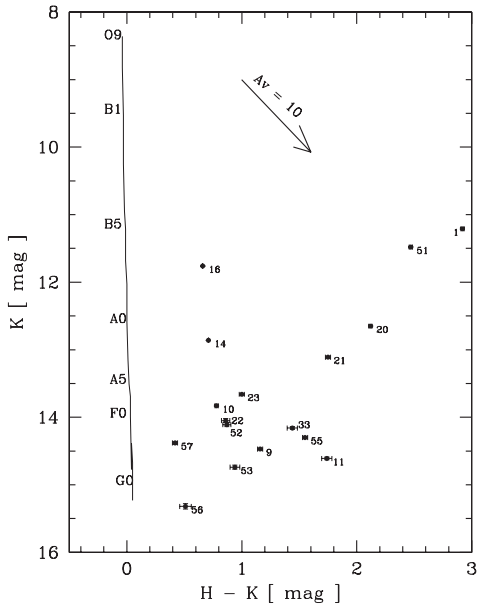

Fig. 5. Near-infrared color–magnitude diagram of objects in the S 255-2 region. The positions of the main-sequence stars (Lang 1992; Wegner 1994) with a distance of 2.4 kpc and a reddening vector are also shown.

YSOs, but infrared nebulae, as discussed in the next section.

3. Discussion

3.1. Two Sets of Bipolar Nebulae

NIRS 20 and NIRS 15 are not stellar, but rather elongated. These structures are most prominent in the K-band, and can also be seen in the H-band. They are probably infrared reflection nebulae associated with bipolar outflows (Tamura et al. 1991). On the other hand, NIRS 3 is bright at K, L', and M' and located between NIRS 20 and NIRS 15. Moreover, NIRS 3 has stellar-like PSFs in L' and M'. Therefore, NIRS 3 is the illuminating source of the reflection nebulae, NIRS 20 and NIRS 15. The elongation of the nebulae is consistent with the outflow direction (along the line joining NIRSs 20, 3, and 15). The outflow direction is consistent with the direction of the large-scale jet by Miralles et al. (1997). A dark lane is located between NIRS 3 and NIRS 20.

Another pair of bipolar nebulae is NIRS 51 and NIRS 15. NIRS 51 does not have a stellar-like PSF, and is slightly elongated. NIRS 51 has no emission in the L'- and M'-bands. Therefore, NIRS 51 is also likely to be an infrared reflection nebula. On the other hand, NIRS 1 is bright and does have a stellar-like PSFs in the L'- and M'-bands. Therefore, we suggest that NIRS 1 and NIRS 51 are not components of a YSO binary, as indicated by Miralles et al. (1997), but NIRS 1 is the illuminating source of both NIRS 51 [as indicated by Tamura et al. (1991)] and NIRS 15.

This scenario is consistent with the polarization pattern of Tamura et al. (1991), in which the polarization vectors in NIRS 15 and NIRS 20 are centrosymmetric around NIRS 3. Also, the polarization pattern, which is not inconsistent with a part of the reflection nebula, is shown at the position of NIRS 51. Tamura et al. (1991) found that the degree of polarization in NIRS 20 is larger than that of NIRS 15. They interpreted this is an effect of the inclination of the bipolar nebula, NIRS 15, being nearer to the Sun than NIRS 20. However, the color of NIRS 15 is redder than NIRS 20, suggesting that NIRS 15 could be more obscured, which appears to be inconsistent with the above simple interpretation. Here, we propose, alternatively, that NIRS 15 is a complex of two reflection nebulae: one is illuminated by NIRS 3 and the other by NIRS 1. High-resolution polarization observations or spectroscopic observations around NIRS 1 are required to confirm this interpretation.

Based on Br γ and $H_2(1–0)$ narrow-band imaging observations, Howard et al. (1997) proposed a "ridge" in the form of an ionized jet originating at NIRS 3 and extending beyond IRS 3 (located out of our field of view) to the northeast. However, in figure 1 there is no extended structure beyond NIRS 20. NIRS 21 and NIRS 33 are not like jet structures but, rather, appear as point sources making a line with NIRSs 20, 3, and 15 by chance.

3.2. Illuminating Sources of the Bipolar Nebulae

As demonstrated above, the illuminating sources of the two sets of bipolar nebulae are NIRS 1 and NIRS 3. These objects, together with bipolar nebulae not well resolved in the previous observations, are as a whole called IRS 1 (Beichman et al. 1979).

NIRS 3 is much brighter at longer wavelengths, and therefore probably extremely embedded. The position of NIRS 3 is coincident with that of S 255-2c at both 5 GHz [$06^h09^m58\overset{s}{.}6+18^\circ00'14\overset{''}{.}0$ (1950)] and at 15 GHz ($06^h09^m58\overset{s}{.}60+18^\circ00'13\overset{''}{.}10$), as well as the position of the source IRS 1 at 20 μm ($06^h09^m58\overset{s}{.}5+18^\circ00'11''$). S 255-2c has a flux of 4.4 ± 0.7 mJy at 5 GHz and 1.97 ± 0.32 mJy at 15 GHz (Rengarajan, Ho 1996). If the spectral index (γ) is defined as $S_\nu \propto \nu^\gamma$, γ is -0.73 ± 0.21 from the ratio of the 15 GHz to the 5 GHz flux densities. This index value is close to the case of an optically thin H II region ($\gamma \sim -0.1$), rather than that of an optically thick H II region ($\gamma \sim +2.0$) or of a stellar wind ($\gamma \sim +0.6$). Thus, we suggest that NIRS 3 is an ultracompact H II region (UCH II). The continuum flux of NIRS 3 at 5 GHz corresponds to a B1 ZAMS star (Snell, Bally 1986; Panagia 1973).

NIRS 1 is another bright source detected in the L'- and M'-bands. However, NIRS 1 is brighter than NIRS 3 in the H-band, and fainter in the L'- and M'-bands, suggesting a smaller amount of extinction than NIRS 3. The magnitudes and colors also suggest that NIRS 1 is intrinsically fainter than NIRS 3. The absence of radio emission at the position of NIRS 1 indicates a spectral type later than B3. Both the intrinsic faintness and late spectral type indicates that NIRS 1 is a less-massive object. The location of NIRS 1 in the color–magnitude diagram (figure 5) is consistent with a deeply embedded B-type star with infrared excess.

3.3. Evolutionary Sequence of Early-B Type Stars

There are several early-B type stars within 10 pc of the S 255 region (see figure 1 of Heyer et al. 1989). The excit-

ing sources of the H II regions (S 254, S 255, and S 257) have been deduced to be B1, B0, and B1 stars from optical intermediate band photometry (Chavarría-K et al. 1987). S 255-1 (G 192.58−0.04, $\sim 1'$ north of S 255-2) is a B0.5 ZAMS star with a UCH II (Snell, Bally 1986). S 255-2a (NIRS 2) and S 255-2b (NIRS 16, IRS 2; Beichman et al. 1979) are estimated to be B1 ZAMS stars (Snell, Bally 1986). The spectral type of S 255-2c (NIRS 3) is also deduced to be B1, as discussed above. Therefore, at least 7 early-B type stars are clustered on this region.

The appearance of these early-B type stars is quite varied. The exciting stars of S 254, S 255, and S 257 are bright at optical wavelengths and display extended H II regions (Chavarría-K et al. 1987). Both S 255-2a and -2b are visible in the Digitized Sky Survey *R* band images, with nebulosity. Their near-infrared colors are not very red, indicating that the sources are moderately embedded ($A_V \sim 15$; Howard et al. 1997). They are not associated with extended H II regions, but have thermal spectra that arise from UCH IIs. S 255-2c is not detected in the optical, *J*, or *H* bands. Its near-infrared color is extremely red, implying that it is deeply embedded. The visual extinction is estimated to be about 60 mag (Howard et al. 1997). S 255-2c has a UCH II, implied by its radio spectrum as well as near-infrared outflows.

The varied appearance of early-B type stars in the S 255 region might suggest a sequence of evolution. An early-B type star might evolve in the following stages: (i) a deeply embedded object with massive outflows and a UCH II; (ii) a moderately embedded object with a UCH II; (iii) an optical star with an extended H II region. As suggested by Heyer et al. (1989) and Howard et al. (1997), star formation in the S 255-2 region may have been triggered by an expansion of nearby H II regions S 255 and S 257. Recently, Fukuda and Hanawa (2000) have numerically simulated star formation triggered by an expansion of H II regions. If the evolved H II regions S 255 and S 257 are the triggers and the UCH IIs S 255-1, -2a, -2b, and -2c are born from the first generation cores, YSOs will be born from the second-generation cores within the next few 10^5 years. FIRS 3, a weak sub-mm and mm peak located $1'$ southeast of S 255-2 (Mezger et al. 1988), may be such a second-generation core.

We are grateful to the Subaru Telescope staff for their support and encouragement. We thank N. Ebizuka, H. Takami, P. Onaka, M. Imanishi, and B. Elms for their support during the construction in CIAO. We also thank I. Shelton for reading the manuscript. Y.I. and Y.N. are supported by the Research Fellowships of the Japan Society for the Promotion of Science for Young Scientists.

References

Beichman, C. A., Becklin, E. E., & Wynn-Williams, C. G. 1979, ApJ, 232, L47
Chavarría-K, C., de Lara, E., & Hasse, I. 1987, A&A, 171, 216
Elias, J. H., Frogel, J. A., Matthews, K., & Neugebauer, G. 1982, AJ, 87, 1029
Evans, N. J., II, Blair, G. N., & Beckwith, S. 1977, ApJ, 217, 448
Fukuda, N., & Hanawa, T. 2000, ApJ, 533, 911
Heyer, M. H., Snell, R. L., Morgan, J., & Schloerb, F. P. 1989, ApJ, 346, 220
Howard, E. M., Pipher, J. L., & Forrest, W. J. 1997, ApJ, 481, 327
Huang, Y.-L., & Thaddeus, P. 1986, ApJ, 309, 804
Jones, T. J., Ashley, M., Hyland, A. R., & Ruelas-Mayorga, A. 1981, MNRAS, 197 413
Koornneef, J. 1983, A&A, 128, 84
Lang, K. R. 1992, Astrophysical Data: Planets & Stars (New York: Springer Verlag)
Lo, K. Y., & Burke, B. F. 1973, A&A, 26, 487
Meyer, M. R., Calvet, N., & Hillenbrand, L. A. 1997, AJ, 114, 288
Mezger, P. G., Chini, R., Kreysa, E., Wink, J. E., & Salter, C. J. 1988, A&A, 191, 44
Miralles, M. P., Salas, L. Cruz-Gonzalez, I., & Kurtz, S. 1997, ApJ, 488, 749
Panagia, N. 1973, AJ, 78, 929
Persson, S. E., Murphy, D. C., Krzeminski, W., Roth, M., & Rieke, M. J. 1998, AJ, 116, 2475
Pipher, J. L., & Soifer, B. T. 1976, A&A, 46, 153
Simon, M., Close, L. M., & Beck, T. L. 1999, AJ, 117, 1375
Snell, R. L., & Bally, J. 1986, ApJ, 303, 683
Rengarajan, T. N., & Ho, P. T. P. 1996, ApJ, 465, 363
Tamura, M., Gatley, I., Joyce, R. R., Ueno, M., Suto, H., & Sekiguchi, M. 1991, ApJ, 378, 611
Tamura, M., Suto, H., Itoh, Y., Ebizuka, N., Doi, Y., Murakawa, K., Hayashi, S. S., & Oasa, Y. 2000, Proc. of SPIE, 4008, 1153
Tokunaga, A. 2000, in Allen's Astrophysical Quantities, ed. A. N. Cox (New York: Springer Verlag), ch. 7
Turner, B. E. 1971, Astrophys. Letter, 8, 73
Wegner, W. 1994, MNRAS, 270, 229